Structure-activity relationship in Ti phosphate-derived photocatalysts for H_2 evolution.

Diego Mateo[a], Francisco Gonell[a], Josep Albero[a], Avelino Corma[a] and Hermenegildo García[a] *

[a] *Instituto de Tecnología Química, Universitat Politècnica de Valéncia-Consejo Superior de Investigaciones Científicas, Avenida de los Naranjos s/n, 46022 Valencia, Spain*

Article history:

Received 26 May 20xx

Revised 9 June 20xx

Accepted 29 June 20xx

Available online

Abstract

Photocatalytic H_2 production has emerged as one of the most clean and promising renewable energy sources. In spite of the efforts to obtain efficient photocatalysts able to produce H_2 from Sun light and water, there is still the need to prepare cheaper and environmental friendlier photocatalysts. Phosphate-based materials could be good candidates to fulfill these requirements. In this manuscript we have prepared a set of mixed Ti^{3+}/Ti^{4+} valence, open-framework titanium phosphates (*of*-$TiPO_4$) and mixed titanium oxide/phosphate derivatives (*cr*-TiP), correlating their structure and composition with the photocatalytic activity for H_2 production. We determined that mixed titanium oxide/phosphate crystalline phases produced enhanced H_2 evolution under Sun simulated light irradiation than mixed Ti^{3+}/Ti^{4+} valence, open-framework titanium phosphates and titanium oxide phases.

Key words: photocatalysis, hydrogen generation, phosphates as semiconductor, visible light photocatalysts

*** Corresponding author.** Tel: +34 96 387 7807; Fax: +34 96 387 7809; E-mail: hgarcia@qim.upv.es

1. Introduction

The photocatalytic conversion of Sunlight into chemical energy has attracted great interest in the last decades due to the need of energy sources alternative to fossil fuels in order to satisfy the increasing

global energy demand, while at the same time reducing CO_2 emission. [1, 2] Since the seminal paper of Fujishima and Honda[3] numerous semiconductor metal oxides have been evaluated as photocatalysts for hydrogen production (TiO_2, ZnO, SnO_2, Fe_2O_3, $SrTiO_3$,etc),[4] but above all, TiO_2 has been the most employed. [5, 6] Although metal oxide-based photocatalysts have shown high photocatalytic efficiency and stability under UV light illumination and they are Earth abundant and non-toxic, they present some important limitations. One of the most difficult to overcome has been the large band gap normally occurring in metal oxides, which determines that absorbed photons having energy larger than the band gap corresponds to the UV zone, which represents less than 5% of the solar irradiance spectrum. [7] Moreover, semiconductors based on metal oxides exhibit large degree of charge recombination, which produces significant losses, reducing drastically the quantum efficiency for hydrogen production. [8]

Different approaches have been developed to overcome these disadvantages, among which modification of the semiconductor with co-catalysts and light harvesters such as noble metals, dyes or different semiconductors have been the most widely studied. [9-12] However, the most efficient co-catalyst are based in expensive noble metals such as Pt, Au, Ag, Ru, Ir, Ni, etc or highly toxic materials (CdS, CdTe or PbS, among others). [13-15] In addition, the incorporation of co-catalysts in metal oxides is carried out with methods based on the chemical reduction of the metal salts, some of them wasting a certain amount of expensive noble metal precursors and limiting photocatalyst production to small batches. For these reasons there is a continued interest in developing new less expensive semiconductor photocatalysts with tunable bandgaps (nitrides, borides, carbides, chalcogenides, etc),[16] able to absorb in the visible region of the solar spectrum, that could be easy to prepare in multigram scale, are non-toxic and are environmentally tolerable.

Phosphate-based materials have recently emerged as good candidates for photocatalytic reactions. [17, 18] Phosphates of first-raw transition metals are widely available and relatively inexpensive materials. In addition, transition metal phosphates present good chemical stability and their band gaps are easy to tune when compared with typical metal oxides. Transition metal phosphates has been already reported as photo(electro)-catalysts for water splitting, pollutant degradation and for some photocatalytic oxidation reactions.[19-21] More recently, Nocera and Kanan described the use of cobalt phosphate decorated electrodes for catalytic oxygen evolution reaction in neutral water [22] and it could be anticipated that their photoexcitation could also lead to interesting activity. Related to the present work,

we have recently reported the visible-light photocatalytic hydrogen production from water methanol mixtures of V-doped, mixed Ti^{3+}/Ti^{4+} valence, open-framework phosphate and Cr-doped open-framework iron phosphate [23, 24] and further studies on the photoactivity of these materials are necessary to fully establish their potential as visible-light photocatalysts.

Besides their use as photoresponsive materials, phosphates can also be the starting precursors of mixed metal oxide/phosphate and other compounds such as phosphides with interesting semiconducting properties. Thus, Schaak and co-workers developed Ni_2P nanoparticles for electrocatalytic hydrogen evolution reaction in acidic media.[25] However, as far as we know there are not yet reports on the photocatalytic activity of materials derived from the thermal chemical reduction of transition metal phosphates.

In the present work, we have prepared and characterized a set of mixed valence (Ti^{3+}/Ti^{+4}), open-framework phosphates and mixed titanium oxide/phosphate derived photocatalysts with the purpose of optimize their activity for hydrogen generation under simulated sun light irradiation in the presence of sacrificial electron donors. Determination of the activity under these optimal conditions will serve to evaluate the potential of these phosphorous containing materials in water splitting by determining the maximum possible efficiency under conditions in which oxygen generation does not limit the process. In fact, continuous H_2 evolution during 24h has been observed for optimized compositions, demonstrating the long-term stability of these mixed materials under reactions conditions. Hydrothermal crystallization has been found a convenient procedure to synthesize open-framework transition metal phosphates in multigram scale. The method also allows doping by adding in the mixture some dopant metal.[23, 24] Chemical reduction of metal phosphates can render some mixed metal oxide/phosphate derivates that could also exhibit interesting photocatalytic activity. Variation of the synthetic conditions in hydrothermal preparation and in the reduction treatment should result in differences in composition and different crystalline phases which should also be reflected in changes in band structure energy and, therefore, in their photocatalytic properties. Herein, the relationship between the different synthetic conditions, structures, compositions of titanium-containing photocatalyst and their activity for hydrogen evolution will be presented.

2. Experimental

2.1. Photocatalyst preparation

Open-framework mixed valence Ti^{3+}/Ti^{4+} phosphate

Titanium metal (Alfa–Aesar, 325 mesh) was mixed with 150 mL of an aqueous solution of 1,3-diaminopropane and phosphoric acid (molar proportion Ti 2: 1,3-diaminopropane 2.21: H_3PO_4 13.65: H_2O 500). The resulting mixture was stirred to achieve a homogeneous suspension and was sealed in a Teflon-lined autoclave. The autoclave was heated in an oven at 170 ^oC during a period varying from 3 to 7 h rendering the materials named *of*-$TiPO_4$-3 and *of*-$TiPO_4$-7, respectively. After the corresponding time, the suspension was cooled down to room temperature and the solid was filtered and exhaustively washed with water, ethanol and acetone. The samples were dried in vacuum at ambient temperature, and stored under inert atmosphere.

Mixed titanium oxide/phosphate synthesis

2.2 mL of $TiCl_4$ (Sigma-Aldrich) was added dropwise to 50 mL of ice/water mixture previously acidified with HCl (pH 2). This solution was added to a solution containing 4.296 g of Na_2HPO_4 (Sigma-Aldrich) dissolved in 50 mL of water. The white slurry obtained was stirred for 10 min, washed with water and centrifuged several times. Finally the precipitates were dried overnight at 100 ^oC.

0.467 g of the above obtained titanium phosphate was grinded with 0.10 g of KBH_4 using an agate mortar until a homogeneous powder was obtained. After that, the mixture was annealed under argon atmosphere at a heating rate of 5 ^oC/min and a hold time of 2 h at 550, 700, 850, 1000 and 1200 ^oC getting the materials named as *cr*-TiP-X (*cr* meaning chemically reduced, cr-TiP-1, *cr*-TiP-2, *cr*-TiP-3, *cr*-TiP-4, *cr*-$TiO_{2,rutile}$, respectively). $(TiO)PO_4$ was prepared by mixing under magnetic stirring 10 ml 0.01 M solutions of $(NH_4)_2(Ti{=}O)C_2O_4$ and Na_2HPO_4 and collecting the solid precipitate that was washed with abundant H_2O until the complete absence of HPO_4^{2-} and dried at 60 ^oC overnight.

2.2. Photocatalyst characterization

XRD patterns were acquired with a Philips Xpert Pro diffractometer in the 2Θ range from 5 to 70 ^{0} using the Cu K_α radiation (λ=1.415 nm) at a rate of 0.5 ^{0}/min. HRTEM images were recorded with a JEM 2100F JEOL 200kV electron microscope. UV-visible absorption spectra were recorded with a Jasco

V-650 spectrophotometer.

2.3. Photocatalytic tests for H_2 production

A suspension of the catalyst (25 mL, 1 $g \times L^{-1}$) was sonicated for 1.5 h and placed in a closed reactor (50 ml) with an irradiation window of 12.56 cm^2. Triethanolamine (TEOA) (15% w/v) (Sigma-Aldrich) was used as sacrificial electron donor. The reactor was placed in a thermostatic bath with a temperature set point of 25 ºC. The suspension was purged with an argon flow of 2 psi for 15 min prior to irradiation to remove oxygen. The photoreaction was performed from the top of the photoreactor by using a solar simulator (Thermo Oriel 1000 W) with an irradiation spot of 100 cm^2 placed at a distance of 10 cm from the top of the photoreactor. The light of the solar simulator was filtered through an Air Mass 1.5 filter and contains approximately 4 % of UV light. The amount of hydrogen collected in the headspace of the reactor was analysed by injecting 100 μL in a gas chromatograph having a MolSieve column, using argon as carrier gas and a TC detector.

3. Results and discussion

3.1. Preparation of titanium-containing photocatalysts

Mixed valence (Ti^{+3}/Ti^{+4}), open framework titanium phosphates (*of*-$TiPO_4$) having different particle size were prepared as described before [23] by hydrothermal crystallization using different synthesis times (*of*-$TiPO_4$-3 and *of*-$TiPO_4$-7). Ti Mixed oxide/phosphate (*cr*-TiP) were prepared starting from titanium phosphate obtained by precipitation and subsequent reduction with KBH_4 at different temperatures (550 ^oC = *cr*-TiP-1, 700 ^oC = *cr*-TiP-2, 850 ^oC = *cr*-TiP-3, 1000 ^oC = *cr*-TiP-4 and 1200 ^oC = *cr*-$TiO_{2,rutile}$) (see experimental section for further details). Scheme 1 summarizes the preparation procedure of the two set of titanium-based phosphorous containing photocatalysts and the list of samples under study.

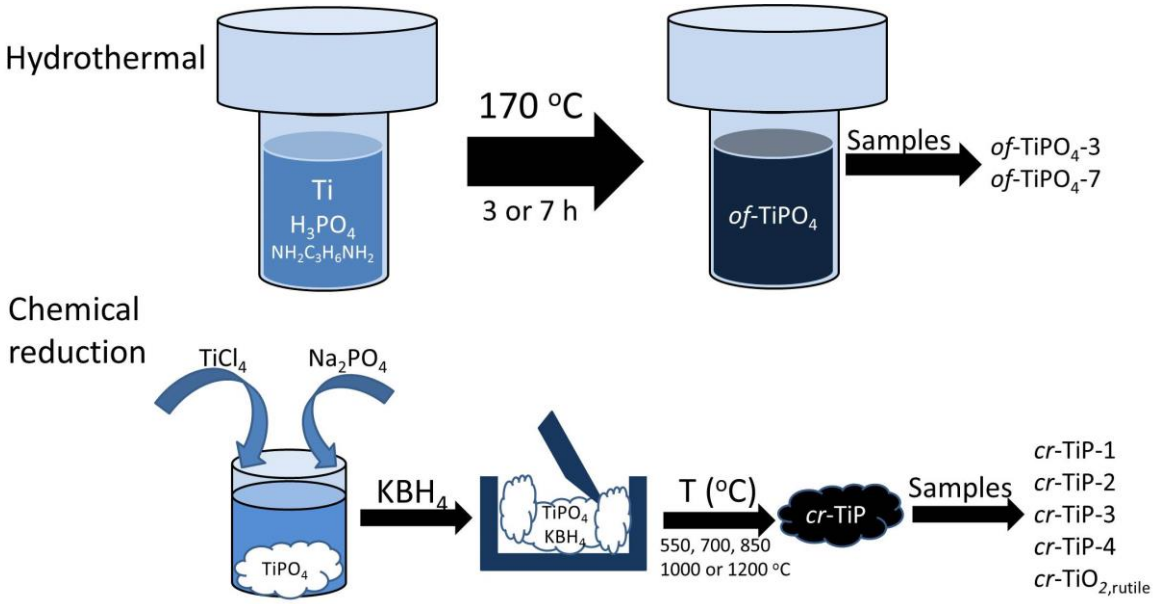

Scheme 1. Preparation procedures titanium based phosphorous containing photocatalyst and list of samples under study.

The as-prepared materials were characterized by X-ray diffraction (XRD), and the diffraction patterns are presented in Figure 1. As can be observed in Figure 1a, the diffraction peaks of samples *of*-$TiPO_4$-3 and *of*-$TiPO_4$-7 agree with those that have been previously reported for mixed Ti^{3+}/Ti^{4+} valence, open-framework phosphates with empirical formula $Ti_2(PO_4)(HPO_4)_2(H_2O)_2$ x $(NH_2CH_2CH_2CH_2NH_2)_{0.5}$.[23] Crystallization time shorter than 3 h resulted in no formation of open-framework formation and the diffraction peaks of the resulting material correspond basically to the unreacted metallic Ti. Even in the case of *of*-$TiPO_4$-3 prepared in 3 h reaction time showed in XRD the presence of residual metallic Ti from the starting reagents, indicating that this reaction time is still not sufficient to allow the complete reaction of all metallic Ti. In contrast, 7 h hydrothermal crystallization ensures the complete oxidation of metallic Ti. In summary, *of*-$TiPO_4$-7 presented pure mixed valence (Ti^{+3}/Ti^{+4}), open-framework crystalline phase, while *of*-$TiPO_4$-3 corresponds to a mixture of mixed valence (Ti^{+3}/Ti^{+4}), open-framework *of*-$TiPO_4$ and metallic Ti with diffraction peaks of similar intensity and for this reason its photocatalytic activity was not studied.

cr-TiP-X samples were prepared by chemical reduction of titanium phosphate by an excess of KBH_4 at high temperatures ranging from 700 to 1200 °C (see experimental section). The corresponding XRD patterns are shown in Figure 1b. As it can be observed at temperatures below 700 °C no crystalline

phases were detected (*cr*-TiP-1). However, between 700 and 1000 ^{o}C a mix of orthorhombic potassium titanium oxide phosphate ($KTiOPO_4$; Ref. pattern 00-035-0802) and tetragonal potassium titanium oxide ($KTi_8O_{16.5}$; Ref. Pattern 00-041-1098) were obtained. Interestingly, potassium incorporation in the solids should occur by reaction with KBH_4 employed as reagent for the chemical reduction procedure. At 700 ^{o}C the intensity of the main peaks of both phases $K(TiO)PO_4$ and $KTi_8O_{16.5}$ located at 28.6^{o} and 27.7^{o}, respectively, were approximately equivalent, being $K(TiO)PO_4$ phase the one with the highest peak intensity. However, when the temperature was increased to 850 ^{o}C, the $K(TiO)PO_4$ peak at 28.6^{o} decreased at expense of the increase of the peak at 27.7^{o} corresponding to $KTi_8O_{16.5}$, indicating that potassium titanium oxide phosphate phase is progressively converted into the potassium titanium oxide phase under reductive treatment. At 1000 ^{o}C $K(TiO)PO_4$ phase practically disappeared and only the $KTi_8O_{16.5}$ phase was present. Higher temperatures (1200 ^{o}C) showed only rutile TiO_2 phase. In order to confirm the presence of the different elements in *cr*-TiP samples, XPS measurements were carried out. Thus, the presence of K, Ti, P and O was detected in *cr*-TiP-700 containing 9.95, 34.2, 6.4 and 49.4 atom%, respectively. In addition, the presence of Ti^{3+}/Ti^{4+} was confirmed as can be observed in Figure 2. In this, the Ti $2p_{3/2}$ XP spectra shows a main peak located at 459 eV, which has been attributed to Ti(IV), while a small shoulder can be observed at 455 eV, indicating the presence of a small amount of Ti(III) as reported before [26]. Actually, the XPS analysis showed that the contribution of Ti(III) is only of 0.7 %. In conclusion, *cr*-TiP samples prepared by chemical reduction of titanium phosphate renders upon heating a mixture of two phases, namely $K(TiO)PO_4$ and $KTi_8O_{16.5}$ in various proportions depending on the reduction temperature. At 700 ^{o}C and 850 ^{o}C, the temperature is not enough for complete removal of phosphate. Higher temperatures promote the formation of pure titanium oxide crystalline phases. Therefore, intermediate temperatures in the range of 700 - 850 ^{o}C render interesting samples with a presence of two phases strongly interacting forming heterojunctions. There are in the literature examples showing that heterojunctions between different titanium materials and phases renders photocatalysts with enhanced H_2 generation activity [23, 27-29].

As a summary of the material synthesis, sufficiently long hydrothermal crystallization provides high quality mixed Ti^{3+}/Ti^{4+} valence, open-framework titanium phosphate crystalline phase and chemical reduction renders a mixture of titanium oxide phosphate and potassium titanate phases when the temperature of the treatment ranges between 700 ^{o}C and 850 ^{o}C. Further reduction temperature induces

complete reduction of phosphates and the conversion of the material into titanium oxide phases, rutile becoming the only detectable crystalline phase at the highest reduction temperature.

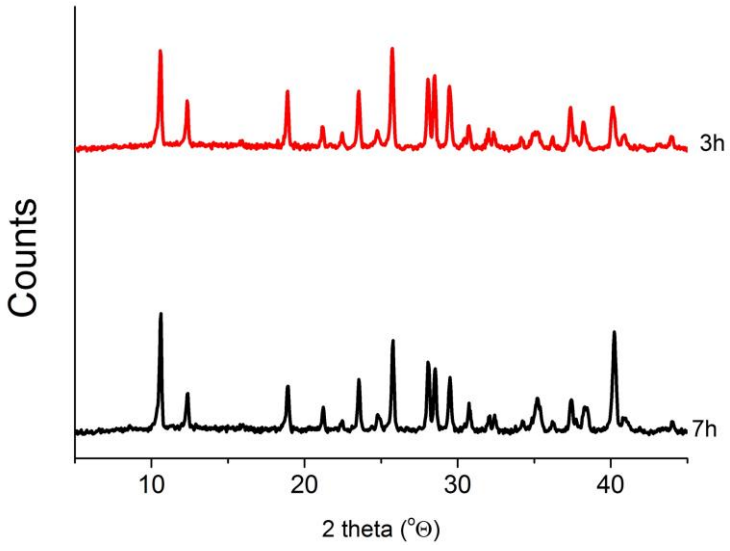

a)

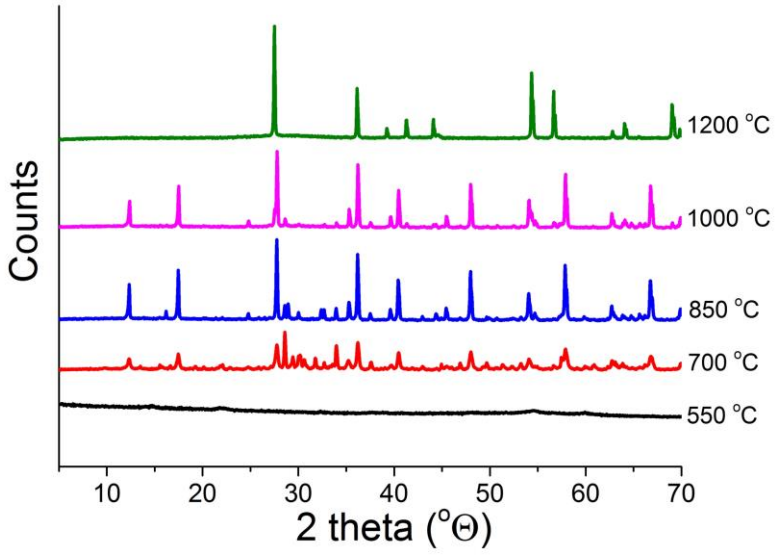

b)

Figure 1. XRD patterns of (a) *of*-$TiPO_4$-3 (red) and *of*-$TiPO_4$-7 (black) samples and (b) *cr*-TiP-1 (black), *cr*-TiP-2 (red), *cr*-TiP-3 (blue), *cr*-TiP-4 (pink) and *cr*-$TiO_{2,rutile}$ (green).

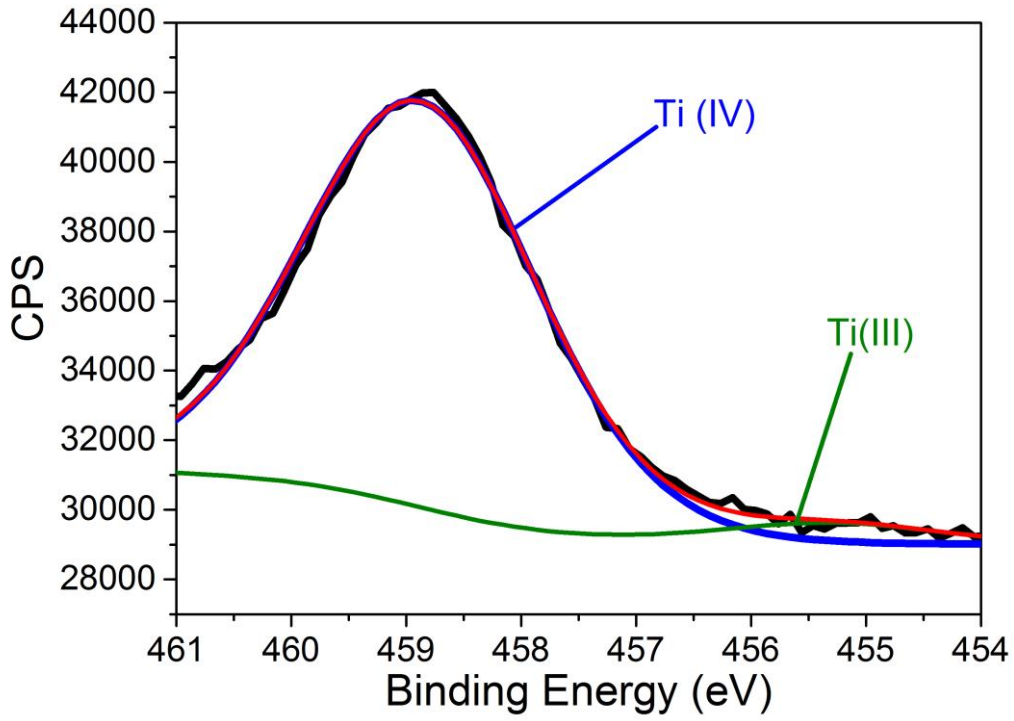

Figure 2. XPS spectra of Ti $2p_{3/2}$ of *cr*-TiP-700 sample.

Transmission electron microscopy (TEM) images of the titanium-containing samples are presented in Figure 3. Very different morphology was found for the two *of*-$TiPO_4$ samples. Surprisingly, *of*-$TiPO_4$-3 sample, with shorter crystallization time, presented bigger sizes than the *of*-$TiPO_4$-7 corresponding to the largest crystallization time. In both cases the presence of small particles forming large agglomerates of 2 and 0.5 µm size approximately for *of*-$TiPO_4$-3 and *of*-$TiPO_4$-7, respectively, was observed. On the other hand, sample *cr*-TiP-1 shows aggregates of approximately 2 µm size lacking defined diffraction electrons, in good agreement with the absence of peaks in XRD. Samples *cr*-TiP-2 and *cr*-TiP-3 present polycrystalline rod-shape particles of 50 - 100 nm width and 1 and 4 µm length for *cr*-TiP-2 and *cr*-TiP-3, respectively. However, *cr*-TiP-4 TEM images showed a completely different morphology constituted by layered particles with a wide range of size distribution, indicating deep structural changes probably reflecting the drastic changes in the composition as consequence of the chemical reduction.

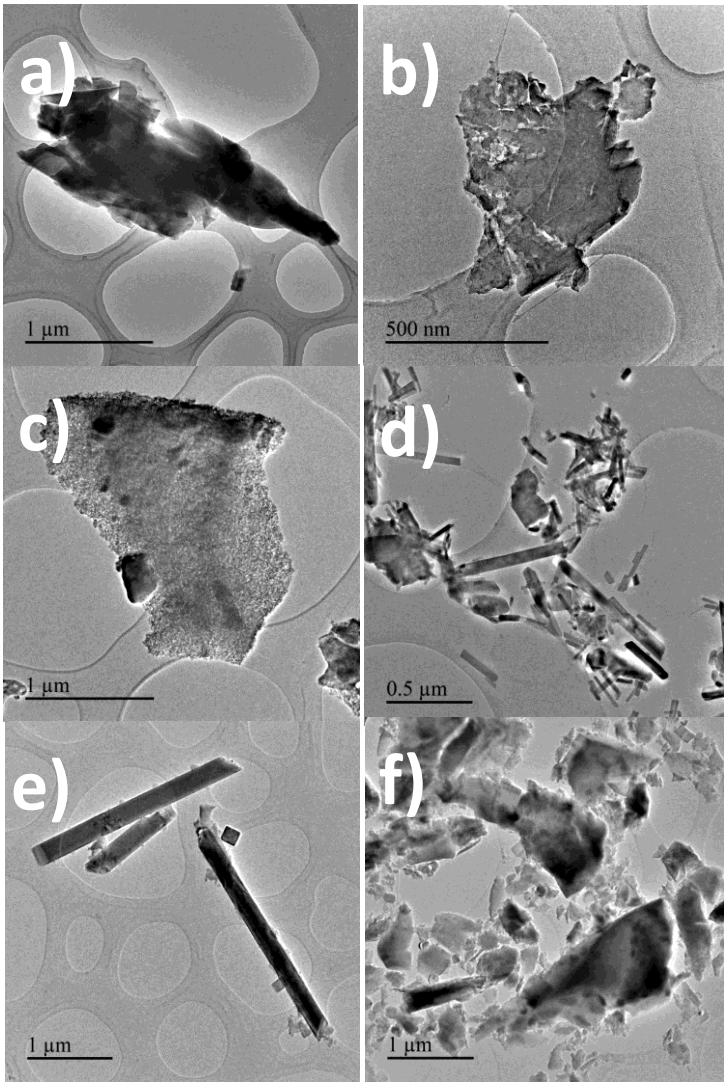

Figure 3. TEM images of samples of *of*-$TiPO_4$-3 (a), *of*-$TiPO_4$-7 (b), *cr*-TiP-1 (c), *cr*-TiP-2 (d), *cr*-TiP-3 (e) and *cr*-TiP-4 (f).

Diffuse reflectance absorption spectra were recorded for all samples and they are presented in Figure 4. *of*-$TiPO_4$-3 and *of*-$TiPO_4$-7 exhibited intense absorption bands in the UV region with two main peaks located at 209 and 269 nm, and 219 and 281 nm, respectively, and a broad band spanning the whole visible range centered at 550 nm. The characteristic feature in the visible region has been previously attributed to the presence of Ti^{3+} ions in the crystalline lattice as consequence of the mixed (Ti^{3+}/Ti^{4+}) valence of titanium ions in *of*-$TiPO_4$.[23] *cr*-TiP-X samples also presented absorption bands in the UV part of the spectra accompanied with broad visible bands. In the case of *cr*-TiP-3 sample a sharp peak centered at 310 nm was present and although *cr*-TiP-2 and *cr*-TiP-4 showed broad shoulders in the same

region a defined band was not recorded. In addition, samples annealed between 700 and 1000 ^{o}C exhibited an increasing broad absorption band which grows in intensity from the visible towards the near infra-red (NIR) (see Figure 4b). This feature could also be a consequence of the presence of some Ti^{3+} ions doping or oxygen vacancies in the existing titanium oxide phase, as it has been reported before. [30, 31] The sample treated at 1200 ^{o}C showed a considerable decrease in the relatively intensity of the visible-NIR absorption, indicating that Ti^{3+} ions or defects in the crystalline framework have disappeared in good agreement with the well crystallized rutile phase. The direct optical band gaps could be calculated from the Tauc plots (see insets Figure 4). *of*-$TiPO_4$ prepared through the hydrothermal method presented direct optical band gaps of 3.57 and 3.45 eV for *of*-$TiPO_4$-3 and *of*-$TiPO_4$-7, respectively. Samples prepared by chemical reduction and annealed at temperatures in the range between 700 and 1000 ^{o}C, the optical band gap decreased from 3.3 to 3.0 eV, for *cr*-TiP-2 and *cr*-TiP-4, respectively, being of 3.27 eV for *cr*-TiP-3. Finally, *cr*-$TiO_{2,rutile}$ presented optical band gap of 3.17 eV, which is close to reported values for rutile TiO_2 band gap.[32]

a)

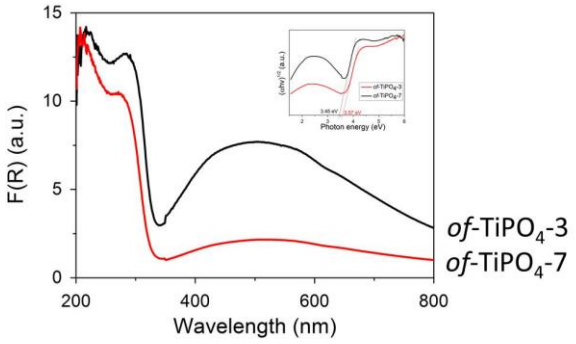

b)

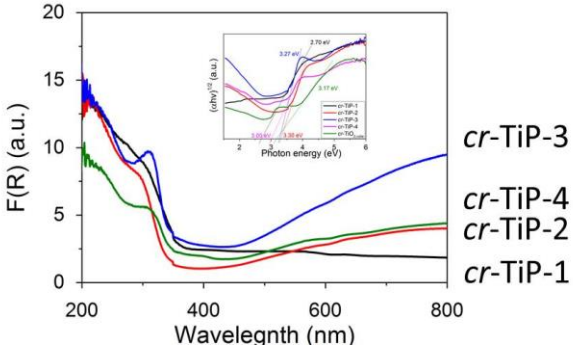

Figure 4. Diffuse reflectance UV-Vis absorption spectra of (a) *of*-$TiPO_4$ and (b) *cr*-TiP samples. The insets show the Tauc's plots obtained from the UV-Vis spectra of the *of*-$TiPO_4$ and *cr*-TiP samples and direct band gap determination.

Emission spectra of the different samples were also recorded, and they are shown in Figure 5. *of*-$TiPO_4$-3 and *of*-$TiPO_4$-7 were excited at 275 nm and both samples showed a main emission band centered at 329 nm and a small shoulder at 466 nm. However, *of*-$TiPO_4$-7 presented two additional shoulders at 390 and 418 nm. The previously commented incorporation of Ti^{3+} in the open-framework structures could have as consequence the appearance of different emission bands at energies lower than those arising from the transition between the edge of the conduction and the valence bands due to the presence of intraband gap states. Emission from trap states in titanium semiconductors has been widely studied and similar emissive properties have been attributed to transition of electrons from the conduction band edge to holes in trapping state located in the band gap.[33]

In the case of *cr*-TiP-1 the emission spectrum was very similar to the sample prepared with hydrothermal method (*of*-$TiPO_4$-3), with a main emission band at 329 nm and a small shoulder located at 460 nm. However, the main photoluminescence bands shifts gradually towards the red depending on the annealing temperatures, being located at 336, 338 and 342 nm for *cr*-TiP-2, *cr*-TiP-3 and *cr*-TiP-4, respectively. Moreover, a second less intense peak at 392 nm starts to develop with temperature. This peak increases in intensity with temperature and it is similar to the one observed in *of*-$TiPO_4$-7 .

a)

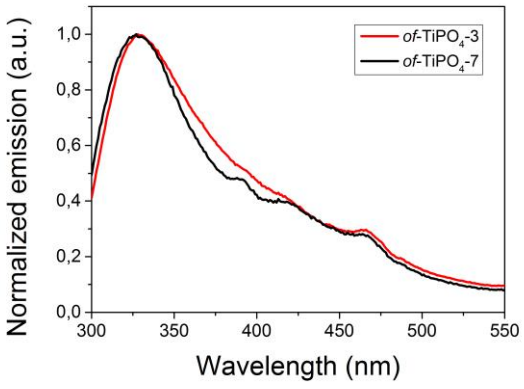

b)

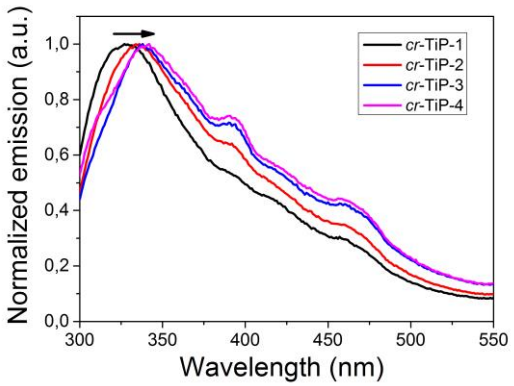

Figure 5. Normalized emission spectra of (a) *of*-$TiPO_4$ and (b) *cr*-TiP samples. Excitation wavelength 275 nm.

Samples exhibiting absorption bands in the visible and NIR region were also excited both at 500 and 600 nm with the aim to detect possible long-wavelength emissions. However, no detectable photoluminescence properties were observed in the range of wavelength available to our equipment (λ<1100 nm).

3.2. Photocatalytic hydrogen generation

The photocatalytic activity of mixed Ti^{3+}/Ti^{4+} valence *of*-$TiPO_4$ for H_2 evolution has been previously reported.[23] Herein we have focused in the comparison of the photocatalytic activity of titanium and phosphorous containing materials prepared at different crystallization times and after chemical reduction affording samples with different composition and crystalline phases, having strong interaction as heterojunctions and therefore, different electronic structures and photocatalytic properties. The proposed mechanism for H_2 production is depicted in Scheme 2. The samples were exposed to sun simulated light irradiation at 1 sun in water/TEOA (15% w:v) at 25 mg/ml concentration and purged with Ar gas for 15 min prior irradiation and the H_2 evolution monitored along time. Figure 6 shows H_2 evolution using samples *cr*-TiP-2, *cr*-TiP-3, *cr*-TiP-4 and *of*-$TiPO_4$-7 as photocatalyst. Samples *cr*-TiP-1 and *cr*-$TiO_{2,rutile}$ have not been included since they did not present any crystalline phase or does not contain phosphorous. *of*-$TiPO_4$-3 was not included in the study due to the presence of metallic Ti. Control experiments using non-reduced *cr*-TiP were performed, but no detectable amounts of H_2 were measured.

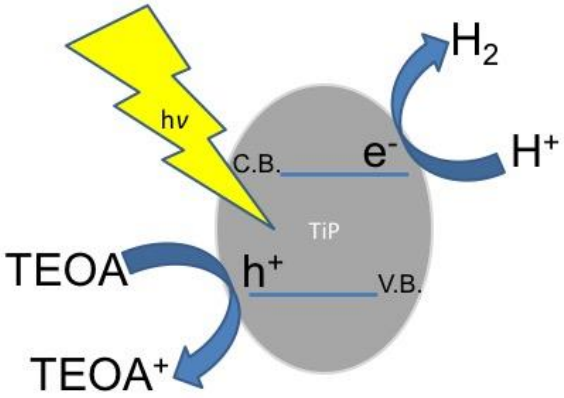

Scheme 2. Proposed mechanism for the photocatalytic H_2 evolution of the phosphorous containing compounds.

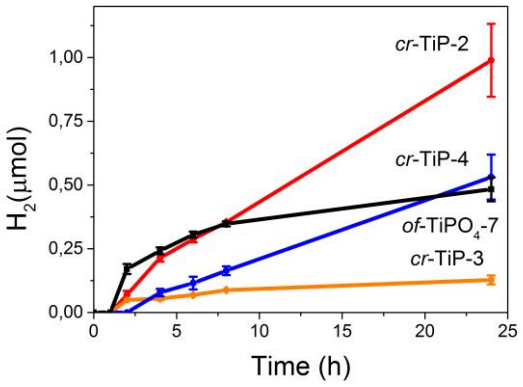

a)

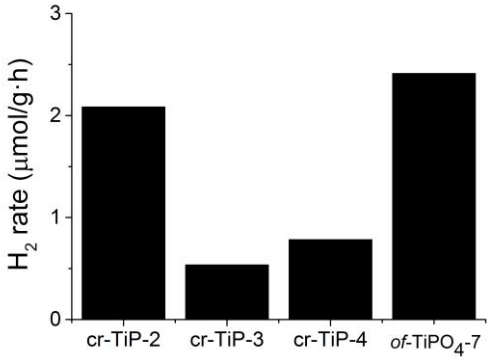

b)

Figure 6. (a) Photocatalytic hydrogen production from water/TEOA mixtures using *cr*-TiP-2 (red), *cr*-TiP-3 (orange), *cr*-TiP-4 (blue) and *of*-$TiPO_4$-7 (black) as photocatalyst under 1 sun simulated light

irradiation. (b) Initial production rate. Experimental conditions 25 ml H_2O/TEOA (15% w:v) and 25 mg of photocatalyst.

As can be observed in Figure 6a, the hydrogen production of *cr*-TiP-2 after 24 h irradiation was approximately twice of *cr*-TiP-4 and *of*-$TiPO_4$-7 at the same time, while *cr*-TiP-3 exhibited the lowest photocatalytic H_2 evolution activity. The quantum efficiencies of the different photocatalyst were calculated and values of $8 \cdot 10^{-4}$, $3.7 \cdot 10^{-4}$, $3.2 \cdot 10^{-4}$ and $1.6 \cdot 10^{-4}$ for *cr*-TiP-2, *cr*-TiP-4, *of*-$TiPO_4$-7 and *cr*-TiP-3, respectively, were obtained. The lowest photocatalytic activity of *cr*-TiP-3 could probably be attributed to its large particle size and the high NIR absorption as consequence of the incorporation of Ti^{3+} in its structure. The increase in particle size usually leads to decrease in catalytic activity as consequence of the decrease in specific surface area. Moreover, the XRD of cr-TiP-3 obtained by reduction at 850 ^{o}C showed that the predominant crystalline phase was $KTi_8O_{16.5}$ without any phosphate, and therefore, we could conclude that the contribution of $K(TiO)PO_4$ in the photocatalytic H_2 evolution could be more relevant than the $KTi_8O_{16.5}$ since the photocatalytic activity of *cr*-TiP-2 containing $K(TiO)PO_4$ is significantly higher than that of *cr*-TiP-4. On the other hand, *cr*-TiP-2 is also more efficient as photocatalyst for H_2 generation than mixed (Ti^{3+}/Ti^{4+}) valence *of*-$TiPO_4$-7 with open-framework structure. Although both preparation methods (hydrothermal and chemical reduction) allowed the obtention of phosphate like materials, the different band structures derived from the different compositions promoted improved H_2 production using the *cr*-TiP-2 sample rather than the *of*-$TiPO_4$-7. Nevertheless, as can be seen in Figure 5b, the initial production rate of *of*-$TiPO_4$-7 was even higher than that of cr-TiP-2, but after this initial period the *of*-$TiPO_4$-7 production rate decreases significantly. It could be that the fresh open-framework mixed Ti^{3+}/Ti^{4+} valence phosphate evolves H_2 with a contribution that is not catalytic, but probably stoichiometric. It is suggested that initial stages of the photocatalytic H_2 evolution should contain a contribution that probably consumes some lower Ti valence until the photocatalyst reaches a stationary state. In contrast, the temporal evolution of H_2 for *cr*-TiP-2 was linear over the full time of the experiment, indicating that its photocatalytic activity is constant and the material is stable under operation conditions. This linear temporal evolution of H_2 is also found for *cr*-TiP-4, but the slope is lower than that observed for *cr*-TiP-2. We can therefore conclude that the heterojunction between $K(TiO)PO_4$ and $KTi_8O_{16.5}$ present in *cr*-TiP-2 should be responsible for the

activity and stability of this photocatalyst that performs better than the open-framework (Ti^{3+}/Ti^{4+}) *of*-$TiPO_4$ phosphate. In a further control (TiO)PO_4 was prepared by precipitation of TiO^{2+} with HPO_4^{2-}, but the resulting pure phosphate did not exhibit photocatalytic activity for H_2 generation. For comparison purposes, the sample *cr*-$TiO_{2,rutile}$, basically composed by TiO_2 in rutile phase and P25 photocatalysts were tested under sun simulated light irradiation, but in both cases negligible photocatalytic activity was demonstrated under this conditions due to the lack of activity in the visible region, as it has been reported before. [20]

4. Conclusions

A series of phosphorous containing titanium photocatalysts have been prepared in a reproducible manner following two different synthetic methods. Hydrothermal crystallization renders pure open-framework TiP crystalline phases after 7 h reaction. Shorter crystallization times resulted in incomplete phosphate formation, the material containing some metallic Ti. Chemical reduction method at high temperature with KBH_4 produced mixed titanium oxide/phosphate that is present in various proportions after annealing at temperatures between 700 ^oC and 1000 ^oC. Lower annealing temperatures did not produce any crystalline phases while, temperatures higher than 1000 ^oC resulted in the formation of titanium oxide. At temperatures above 1000 ^oC only titanium oxide crystalline phase was found. It was observed that mixed titanium oxide/phosphate obtained with the chemical reduction method from titanium phosphate at 700 ^oC produced a stable photocatalyst that exhibits the highest H_2.

Acknowledgments

Financial support by the Spanish Ministry of Economy and competitivenes (CIQ2015-69153-C2-1-R) is gratefully acknowledged.

References:

[1] A. Listorti, J. Durrant, J. Barber, Artificial photosynthesis: Solar to fuel, Nat Mater, 8 (2009) 929-930.
[2] N. Armaroli, V. Balzani, The Future of Energy Supply: Challenges and Opportunities, Angewandte Chemie International Edition, 46 (2007) 52-66.
[3] A. Fujishima, K. Honda, Electrochemical Photolysis of Water at a Semiconductor Electrode, Nature, 238

(1972) 37-38.
[4] K. Maeda, Photocatalytic water splitting using semiconductor particles: History and recent developments, Journal of Photochemistry and Photobiology C: Photochemistry Reviews, 12 (2011) 237-268.
[5] M. Ni, M.K.H. Leung, D.Y.C. Leung, K. Sumathy, A review and recent developments in photocatalytic water-splitting using for hydrogen production, Renewable and Sustainable Energy Reviews, 11 (2007) 401-425.
[6] A. Fujishima, T.N. Rao, D.A. Tryk, Titanium dioxide photocatalysis, Journal of Photochemistry and Photobiology C: Photochemistry Reviews, 1 (2000) 1-21.
[7] J. Schneider, M. Matsuoka, M. Takeuchi, J. Zhang, Y. Horiuchi, M. Anpo, D.W. Bahnemann, Understanding TiO2 Photocatalysis: Mechanisms and Materials, Chemical Reviews, 114 (2014) 9919-9986.
[8] N. Serpone, D. Lawless, R. Khairutdinov, E. Pelizzetti, Subnanosecond Relaxation Dynamics in TiO2 Colloidal Sols (Particle Sizes Rp = 1.0-13.4 nm). Relevance to Heterogeneous Photocatalysis, The Journal of Physical Chemistry, 99 (1995) 16655-16661.
[9] C.N.R. Rao, S.R. Lingampalli, Generation of Hydrogen by Visible Light-Induced Water Splitting with the Use of Semiconductors and Dyes, Small, 12 (2016) 16-23.
[10] S. Martha, P. Chandra Sahoo, K.M. Parida, An overview on visible light responsive metal oxide based photocatalysts for hydrogen energy production, RSC Advances, 5 (2015) 61535-61553.
[11] Y. Xu, B. Zhang, Hydrogen photogeneration from water on the biomimetic hybrid artificial photocatalytic systems of semiconductors and earth-abundant metal complexes: progress and challenges, Catalysis Science & Technology, 5 (2015) 3084-3096.
[12] B. Xiao, M. Zhu, X. Li, P. Yang, L. Qiu, C. Lu, A stable and efficient photocatalytic hydrogen evolution system based on covalently linked silicon-phthalocyanine-graphene with surfactant, International Journal of Hydrogen Energy, 41 (2016) 11537-11546.
[13] Y. Ma, X. Wang, Y. Jia, X. Chen, H. Han, C. Li, Titanium Dioxide-Based Nanomaterials for Photocatalytic Fuel Generations, Chemical Reviews, 114 (2014) 9987-10043.
[14] X. Li, J. Yu, J. Low, Y. Fang, J. Xiao, X. Chen, Engineering heterogeneous semiconductors for solar water splitting, Journal of Materials Chemistry A, 3 (2015) 2485-2534.
[15] K. von Allmen, R. Moré, R. Müller, J. Soriano-López, A. Linden, G.R. Patzke, Nickel-Containing Keggin-Type Polyoxometalates as Hydrogen Evolution Catalysts: Photochemical Structure–Activity Relationships, ChemPlusChem, 80 (2015) 1389-1398.
[16] F.E. Osterloh, Inorganic nanostructures for photoelectrochemical and photocatalytic water splitting, Chemical Society Reviews, 42 (2013) 2294-2320.
[17] D.J. Martin, G. Liu, S.J.A. Moniz, Y. Bi, A.M. Beale, J. Ye, J. Tang, Efficient visible driven photocatalyst, silver phosphate: performance, understanding and perspective, Chemical Society Reviews, 44 (2015) 7808-7828.
[18] T. Wu, S. Chen, D. Zhang, J. Hou, Facile preparation of semimetallic MoP2 as a novel visible light driven photocatalyst with high photocatalytic activity, Journal of Materials Chemistry A, 3 (2015) 10360-10367.
[19] M.P. Kapoor, S. Inagaki, H. Yoshida, Novel Zirconium−Titanium Phosphates Mesoporous Materials for Hydrogen Production by Photoinduced Water Splitting, The Journal of Physical Chemistry B, 109 (2005) 9231-9238.
[20] J.C. Yu, L. Zhang, Z. Zheng, J. Zhao, Synthesis and Characterization of Phosphated Mesoporous Titanium Dioxide with High Photocatalytic Activity, Chemistry of Materials, 15 (2003) 2280-2286.
[21] X. Wang, H. Pang, S. Zhao, W. Shao, B. Yan, X. Li, S. Li, J. Chen, W. Du, Ferric Phosphate Hydroxide

Microcrystals for Highly Efficient Visible-Light-Driven Photocatalysts, ChemPhysChem, 14 (2013) 2518-2524.
[22] M.W. Kanan, D.G. Nocera, In Situ Formation of an Oxygen-Evolving Catalyst in Neutral Water Containing Phosphate and Co2+, Science, 321 (2008) 1072-1075.
[23] M. Serra, H.G. Baldovi, F. Albarracin, H. Garcia, Visible light photocatalytic activity for hydrogen production from water–methanol mixtures of open-framework V-doped mixed-valence titanium phosphate, Applied Catalysis B: Environmental, 183 (2016) 159-167.
[24] M. Serra, H.G. Baldovi, M. Alvaro, H. Garcia, Doped Framework Iron Hydroxyl Phosphate as Photocatalyst for Hydrogen Production from Water/Methanol Mixtures, European Journal of Inorganic Chemistry, 2015 (2015) 4237-4243.
[25] E.J. Popczun, J.R. McKone, C.G. Read, A.J. Biacchi, A.M. Wiltrout, N.S. Lewis, R.E. Schaak, Nanostructured Nickel Phosphide as an Electrocatalyst for the Hydrogen Evolution Reaction, Journal of the American Chemical Society, 135 (2013) 9267-9270.
[26] T.-D. Pham, B.-K. Lee, D. Pham-Cong, Advanced removal of toluene in aerosol by adsorption and photocatalytic degradation of silver-doped TiO2/PU under visible light irradiation, RSC Advances, 6 (2016) 25346-25358.
[27] S.-y. Guo, S. Han, B. Chi, J. Pu, J. Li, Synthesis of shape-controlled mesoporous titanium phosphate nanocrystals: The hexagonal titanium phosphate with enhanced hydrogen generation from water splitting, International Journal of Hydrogen Energy, 39 (2014) 2446-2453.
[28] X. Chen, L. Liu, P.Y. Yu, S.S. Mao, Increasing Solar Absorption for Photocatalysis with Black Hydrogenated Titanium Dioxide Nanocrystals, Science, 331 (2011) 746-750.
[29] E. Borgarello, J. Kiwi, M. Graetzel, E. Pelizzetti, M. Visca, Visible light induced water cleavage in colloidal solutions of chromium-doped titanium dioxide particles, Journal of the American Chemical Society, 104 (1982) 2996-3002.
[30] F. Zuo, K. Bozhilov, R.J. Dillon, L. Wang, P. Smith, X. Zhao, C. Bardeen, P. Feng, Active Facets on Titanium(III)-Doped TiO2: An Effective Strategy to Improve the Visible-Light Photocatalytic Activity, Angewandte Chemie International Edition, 51 (2012) 6223-6226.
[31] F. Zuo, L. Wang, T. Wu, Z. Zhang, D. Borchardt, P. Feng, Self-Doped Ti3+ Enhanced Photocatalyst for Hydrogen Production under Visible Light, Journal of the American Chemical Society, 132 (2010) 11856-11857.
[32] M. Landmann, E. Rauls, W.G. Schmidt, The electronic structure and optical response of rutile, anatase and brookite TiO 2, Journal of Physics: Condensed Matter, 24 (2012) 195503.
[33] H.N. Ghosh, S. Adhikari, Trap State Emission from TiO2 Nanoparticles in Microemulsion Solutions, Langmuir, 17 (2001) 4129-4130.